Electronic Supporting Information(ESI)

Visible Light-Driven Highly-Efficient Hydrogen Production by a Naphthalene Imide Derivative-Sensitized TiO_2 Photocatalyst

Dan Wei,[a] Kang Yang,[a] Chunman Jia*[a] and Jianwei Li *[b]

[a.] *Hainan Provincial Key Laboratory of Fine Chem, School of Chemical Engineering and Technology, Hainan University, Haikou 570228, China. E-mail: jiachunman@hainanu.edu.cn*

[b.] *MediCity Research Laboratory, University of Turku, Tykistökatu 6, FI-20520 Turku, Finland. E-mail: jianwei.li@utu.fi*

Contents

1 Experimental

1.1 Synthetic procedures of compound DT

1.1.1 Synthesis of Compound 1.[S1]

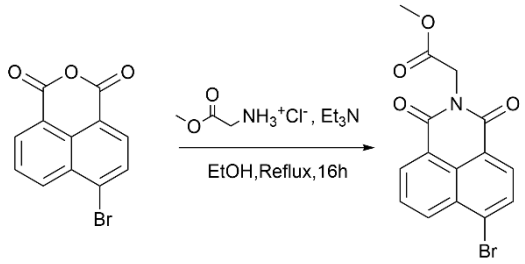

1

4-bromo-1,8-naphthalic anhydride (1.00 g, 3.61 mmol) and methyl glycinate hydrochloride (0.90 g, 7.22 mmol) were added to absolute ethanol (25 mL) and refluxed at 105 °C after dropwise addition of triethylamine (0.50 mL, 3.61 mmol) for 16 h. TLC monitoring is followed by cooling to room temperature, filtering to collect the pellet and repeatedly washing with ethanol until the rinse solution is colorless, then drying under vacuum (1.97 g，78%)。^{1}H NMR (400 MHz, $CDCl_3$) δ 8.67 (d, J = 6.1 Hz, 1H), 8.60 (d, J = 8.5 Hz, 1H), 8.43 (d, J = 7.9 Hz, 1H), 8.05 (d, J = 7.9 Hz, 1H), 7.89 – 7.84 (m, 1H), 4.95 (s, 2H), 3.79 (s, 3H).

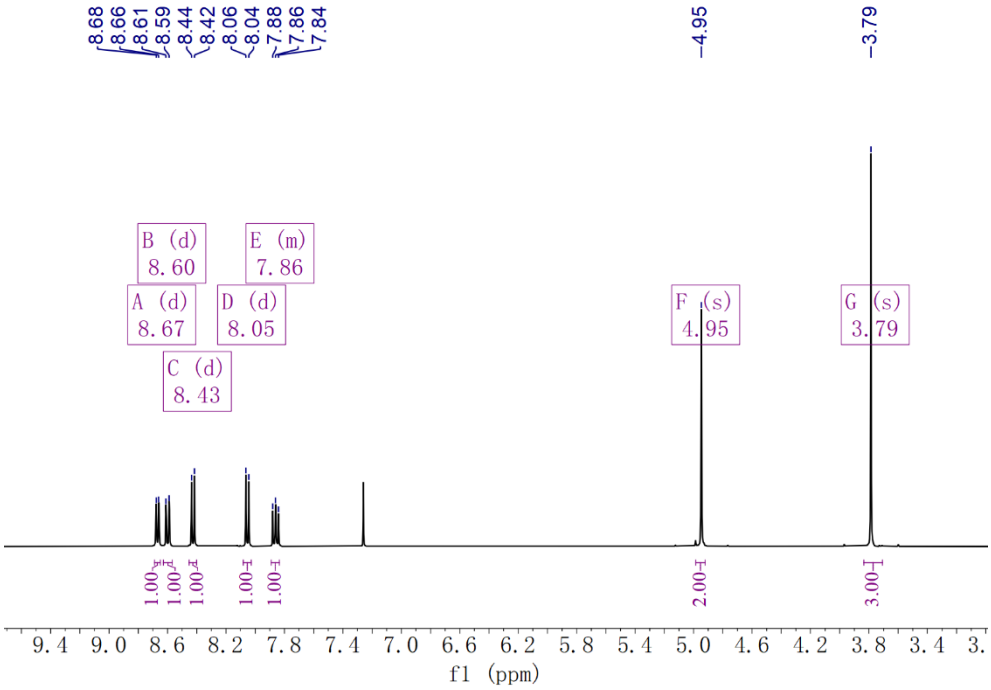

Fig. S1 ^{1}H NMR of Compound **1** in $CDCl_3$.

1.1.2 Synthesis of Compound 2.

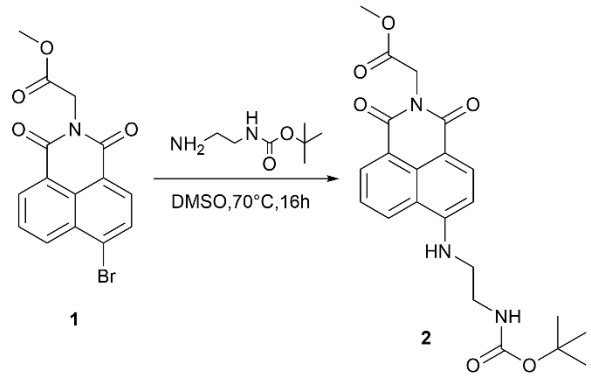

Compound **1** (0.85 g, 2.46 mmol) was dissolved in DMSO (4 mL), mono-Boc ethylenediamine (1.18 mL, 7.38 mmol) was added dropwise, the solution immediately turned pink and stirred at 70 °C for 16 h. After the end of the reaction, cool to room temperature, neutralize the pH with dilute HCl aqueous solution to generate a precipitate, dilute the solution with dichloromethane, and then wash with water. After drying the organic phase with anhydrous Na_2SO_4, at least a residual amount is evaporated under vacuum. Add a large amount of ice-cold n-hexane to precipitate the product as an orange solid, collect and dry under vacuum (1.05 g, quantitative). ^{1}H NMR (400 MHz, $CDCl_3$) δ 8.54 (d, J = 7.4 Hz, 1H), 8.43 (d, J = 8.5 Hz, 1H), 8.28 (d, J = 8.5 Hz, 1H), 7.61 – 7.56 (m, 1H), 6.57 (d, J = 8.5 Hz, 1H), 4.95 (s, 2H), 3.77 (s, 3H), 3.63 (s, 2H), 3.45 (t, J = 5.1 Hz, 2H), 1.48 (s, 9H).

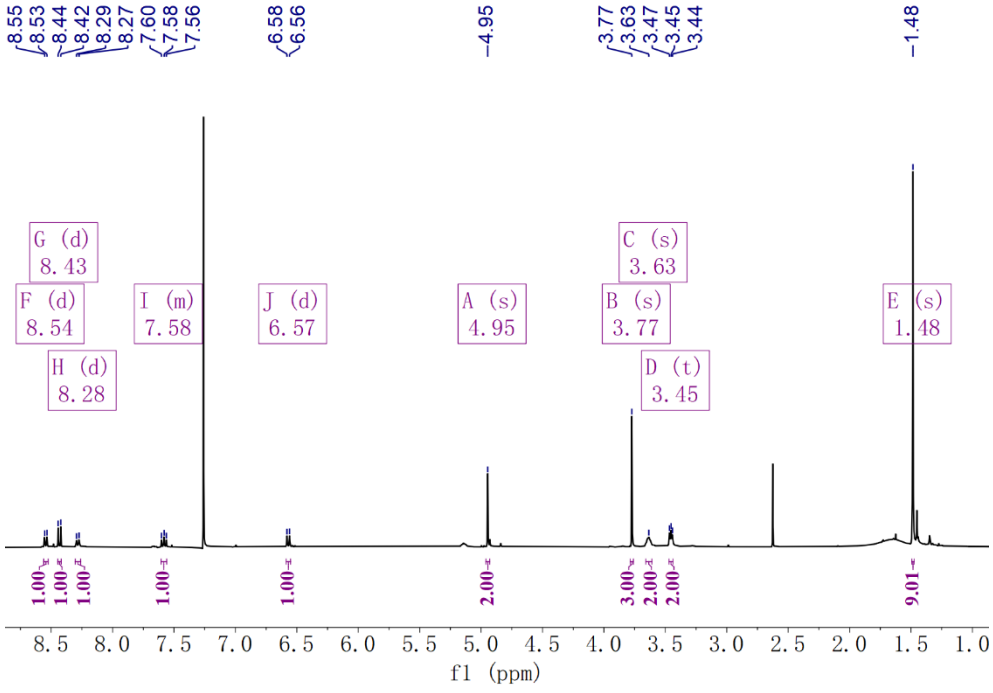

Fig. S2 ^{1}H NMR of Compound 2 in $CDCl_3$.

1.1.3 Synthesis of Compound 3.

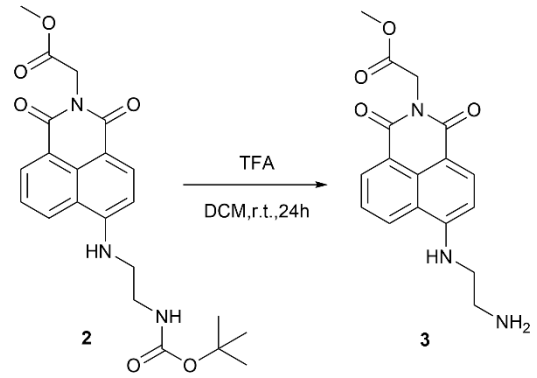

Compound **2** (0.78 g, 1.83 mmol) was completely dissolved in ultra-dry dichloromethane (3 mL), trifluoroacetic acid (2.61 mL) was added dropwise and stirred for 24 h at room temperature protected from light. After the end of the reaction, the pH is neutralized to 8-9 with saturated $NaHCO_3$ solution and a precipitate is generated, the product is extracted from water with DCM, and the organic layer is dried with anhydrous Na_2SO_4. The solvent is then removed by vacuum to obtain a yellow solid (0.12 g, 20%). ^{1}H NMR (400 MHz, MeOD) δ 8.51 – 8.38 (m, 2H), 8.27 (d, J = 8.6 Hz, 1H), 7.62 – 7.55 (m, 1H), 6.77 (d, J = 8.6 Hz, 1H), 4.85 (s, 2H), 3.77 (s, 3H), 3.52 (t, J = 6.4 Hz, 2H), 3.04 (t, J = 6.4 Hz, 2H).

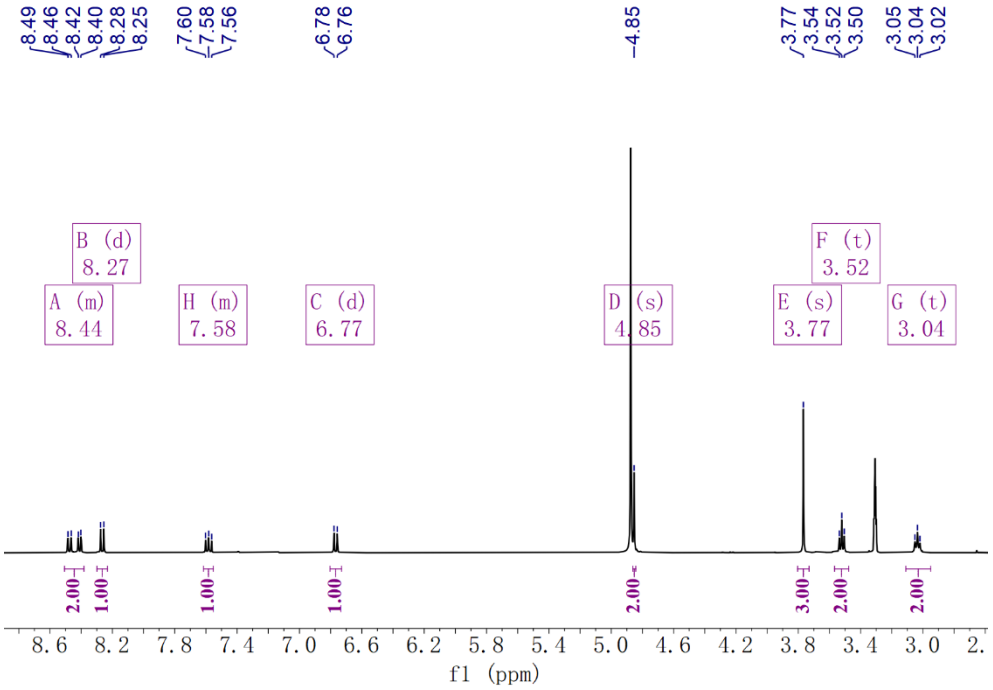

Fig. S3 ^{1}H NMR of Compound 3 in MeOD.

1.1.4 Synthesis of Compound DT.[S2, 3]

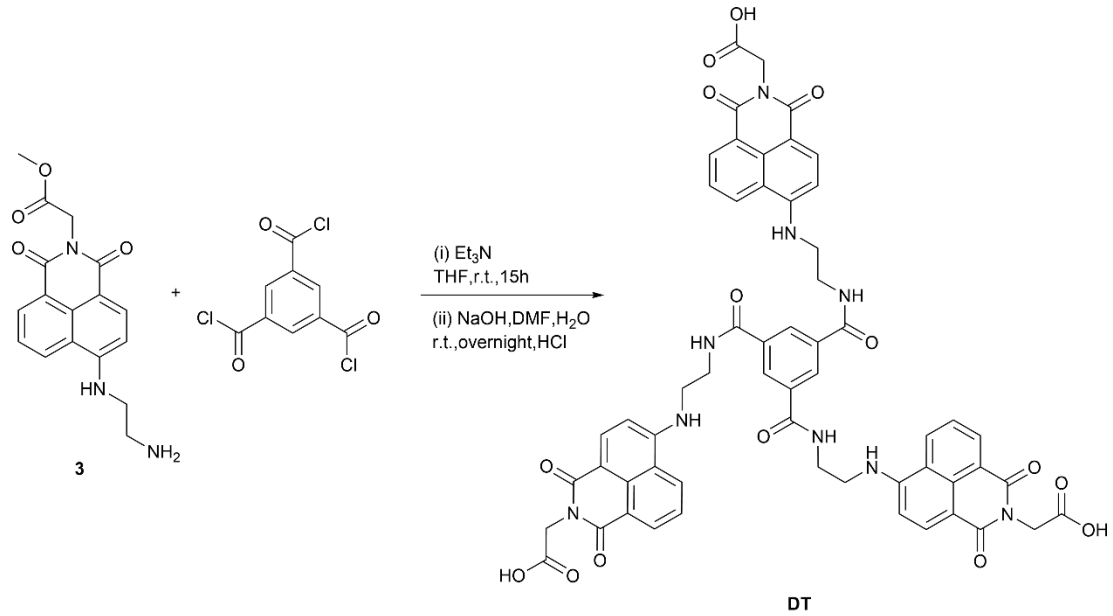

A solution of 1,3,5-benzenetricarboxylic acid chloride (0.09 mmol, 0.024 g) in ultra-dry THF was gradually added to a solution of compound **3** (0.367 mmol, 0.12 g) and triethylamine (0.1 mL) in ultra-dry THF. The mixture was stirred at room temperature for 15 h. After completion of the reaction, the solvent was removed and the residue was recrystallized in DMF and ethanol, washed with ethanol and water, and filtered to dry(0.05 g, 62%). Next, a solution of NaOH (0.75 mmol, 0.03 g) in water (1 mL) was slowly added to the DMF (4 mL) solution of the above drying product (0.057 mmol, 0.065 g), and the mixture was stirred overnight at room temperature. The pH of the reaction mixture was adjusted to acidic by adding dilute hydrochloric acid, resulting in the precipitation of the product. The product was collected and dried under vacuum (0.056 g, 90%). ^{1}H NMR (400 MHz, DMSO) δ 8.70 (d, J = 7.8 Hz, 3H), 8.53 (s, 3H), 8.46 (d, J = 8.3 Hz, 3H), 8.30 (d, J = 8.5 Hz, 3H), 8.05 (s, 3H), 7.75 – 7.70 (m, 3H), 6.99 (d, J = 8.8 Hz, 3H), 4.69 (s, 6H), 3.64 (s, 12H). ^{13}C NMR (101 MHz, DMSO) δ 170.54, 166.17, 163.99, 163.05, 151.25, 135.02, 131.27, 129.96, 129.46, 121.96, 120.68, 104.33, 41.83, 38.51. MS: m/z: calcd: 1094.2962; found: 1094.2957[M-H^{+}].

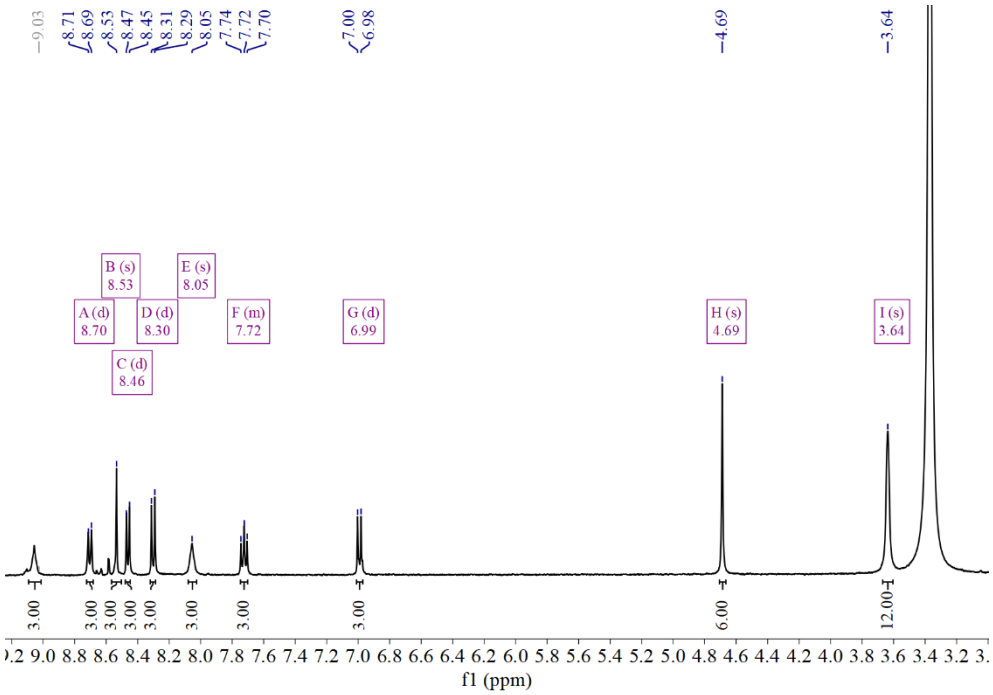

Fig. S4 ^{1}H NMR of Compound DT in d_6-DMSO.

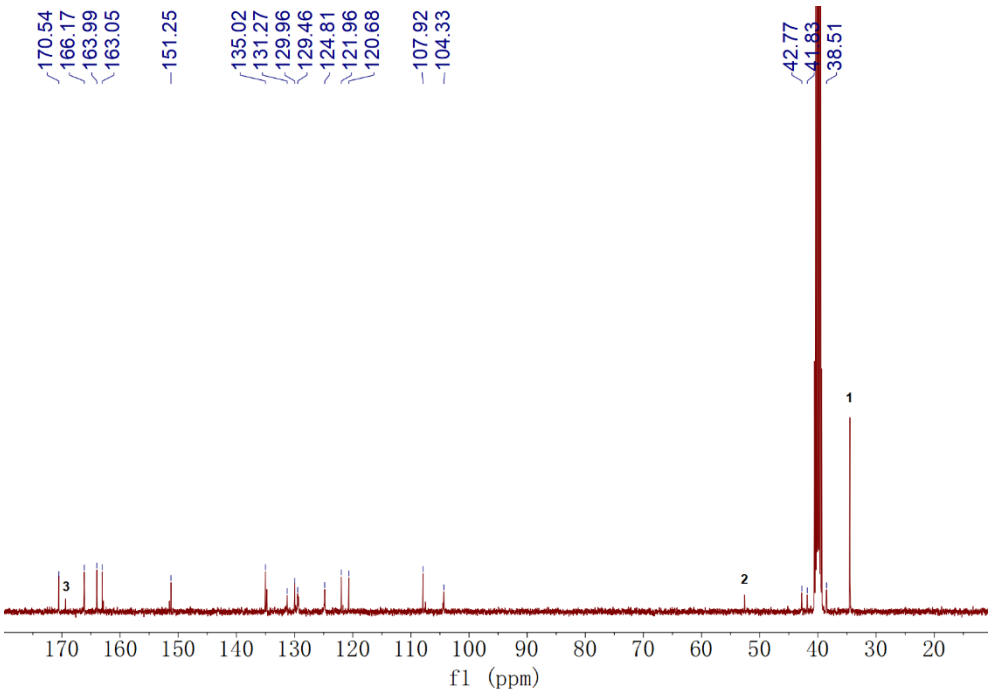

Fig. S5 ^{13}C NMR of Compound **DT** in d_6-DMSO,in which the peaks 1,2,3 are assigned to the residual solvent *N*,*N*-Dimethylformamide(DMF**).**

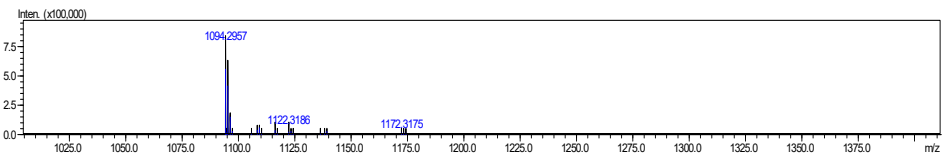

Fig. S6 HRMS of Compound DT.

1.2 Synthesis procedure of composite materials

1.2.1 Synthesis of DT-TiO_2 by sol-gel method.[S4]

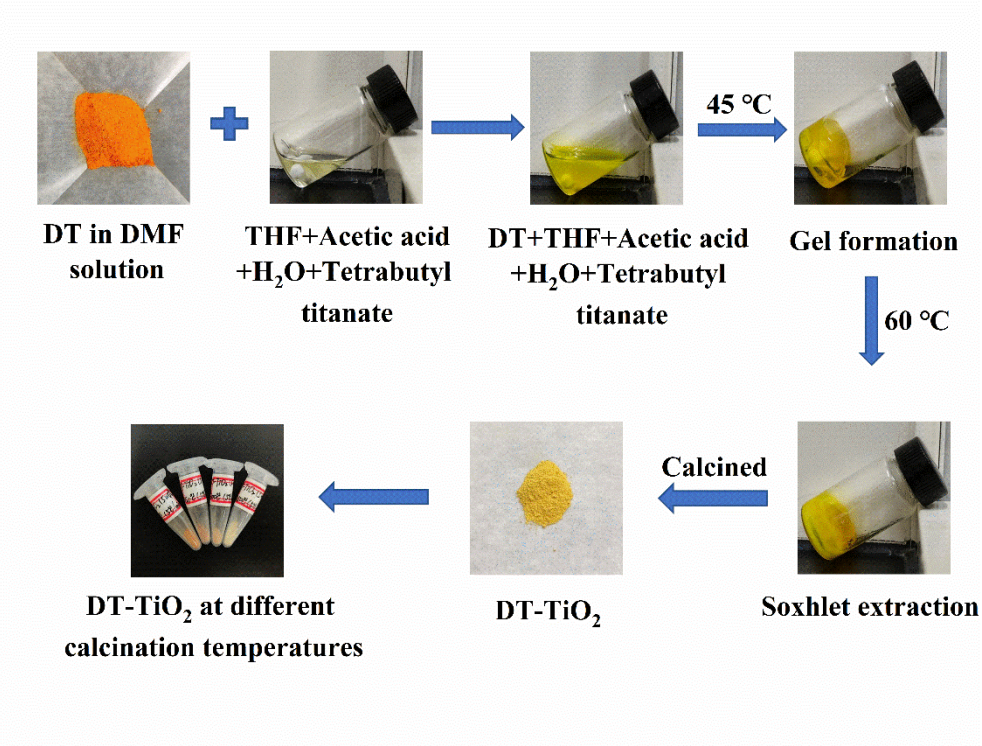

Fig. S7 Synthetic procedure of the hybrid DT-TiO_2 materials.

The detailed synthesis process of DT-TiO_2 is illustrated in Fig. S7. The sol-gel method was employed for the synthesis. First, a 20 mL sample bottle was placed in a heating module, and ultra-dry tetrahydrofuran (1 mL), glacial acetic acid (168 μL), distilled water (106 μL), and tetrabutyl titanate (1 mL) were sequentially added under stirring at room temperature. Subsequently, the DT solution dissolved in ultra-dry DMF (1 mL) was rapidly added to the sample bottle. The solution turned from transparent to yellow, and the temperature was gradually increased to 45 °C. The mixture was heated and stirred until it formed a gel.

The gel was placed in a vacuum oven at 60 °C overnight for complete drying, resulting in a yellow solid. This solid was then ground into a powder and subjected to a Soxhlet extraction with distilled water for 2 days to remove impurities. Afterward, the sample was dried in a vacuum oven at 45 °C and calcined in a tube furnace with programmed temperature increase, followed by natural cooling to obtain a yellow-brown powder.

Materials prepared at different calcination temperatures (200°C, 250 °C, 300 °C, and 350 °C) were designated as DT-TiO_2 (200 °C), DT-TiO_2 (250 °C), DT-TiO_2 (300 °C), and DT-TiO_2 (350 °C). TiO_2 and other hybrid materials synthesized under different conditions were named using similar methods.

1.2.2 Synthesis of Pt@DT-TiO_2 composites

Disperse 10 mg of DT-TiO_2(5.0 wt%) material in a solution of 10 mL H_2O and 8 mL methanol. Add varying amounts (30 μL, 60 μL, 100 μL, 150 μL, and 200 μL) of K_2PtCl_4

solution (2.13 mg/mL) and stir the mixture in vacuum for 1 hour. Conduct in-situ photochemical deposition under full light irradiation from a 300 W xenon lamp. After centrifugation and vacuum drying, Pt@DT-TiO_2 (0.3 wt%, 0.6 wt%, 1.0 wt%, 1.5 wt%, and 2.0 wt%) samples are obtained. The loading of Pt is analyzed using inductively coupled plasma atomic emission spectrometry.

2 Materials and methods

2.1 Characterization method

The compound was fully dissolved in deuterated solvent, and a Bruker 400 MHz nuclear magnetic resonance spectrometer was employed to obtain the ^{1}H NMR and ^{13}C NMR spectra. The mass spectra (MS) were measured using a Shimadzu LCMS-IT-TOF ion trap-time-of-flight liquid mass spectrometer. Infrared spectra were obtained using a Nicolet IS50 Fourier Transform Infrared Spectrometer by mixing dry solid samples with potassium bromide and grinding them into tablets. UV-Vis absorption was measured using a Shimadzu UV-2600 UV-Vis spectrophotometer, and fluorescence tests were conducted on a HORIBA FluoroLog-3 high-sensitivity fluorescence spectrometer. Thermogravimetric analysis was performed with a NETZSCH STA 449F5 thermogravimetric analyzer under an air atmosphere (humidity 76%), heating from 30 °C to 600 °C at a rate of 10 °C/min. X-ray diffraction (XRD) was measured using a Bruker D8 ADVANCE X-ray diffractometer. The Pt loading test was conducted with an Agilent ICPOES730 inductively coupled plasma atomic emission spectrometer (ICP-AES). Scanning electron microscope (SEM) images were obtained using a Gemini300 instrument, while transmission electron microscopy (TEM), high-resolution TEM, selected area electron diffraction, and EDX images were acquired using a FEI Talos F200X TEM at an accelerating voltage of 200 kV. X-ray photoelectron spectroscopy (XPS) measurements were taken with a Thermo escalab 250Xi instrument. Physical adsorption tests were conducted using an ASAP 2460 physical adsorption analyzer, with N_2 adsorption and desorption at 77 K, and degassing at 250 °C for 8 hours. All electrochemical tests were performed on an IVIUMnSTAT electrochemical workstation using a three-electrode system, with platinum as the counter electrode, Ag/AgCl as the reference electrode, and 0.5 M Na_2SO_4 as the electrolyte. A 300 W xenon lamp with a 400 nm cut-off filter was employed as the light source for Mott-Schottky, instantaneous photocurrent response, and electrochemical impedance tests. The working electrode was prepared as follows: The sample to be tested was dispersed in 0.5 mL of a mixed solution of ethanol and nafion. After sufficient ultrasonic dispersion, the sample was deposited onto FTO conductive glass to form a 0.25 cm^2 film.

2.2 Photocatalytic test method

The hydrogen production system utilized in the photocatalytic hydrogen production test is the Perfect Light Lab Solar-6A, and the hydrogen amount is measured using a Fuli 9790II gas chromatograph. The photocatalytic water splitting hydrogen production reaction is carried out in a glass reactor with a quartz cover connected to a closed gas cycle, which is purged with high-purity Ar_2 before illumination. Disperse 10 mg of photocatalyst material in 20 mL of water/triethanolamine solution (volume ratio 9:1) with continuous stirring. Cool the mixture to 5 °C using circulating cooling water, and then expose it to irradiation from a 300 W xenon lamp, filtering out the ultraviolet light. On-line gas chromatography is employed to measure the hydrogen evolution amount at 1-hour intervals.

3 Photocatalytic hydrogen production

To evaluate the photocatalytic activity of the material under visible light irradiation, we studied the effect of different DT contents(0, 2.5, 5.0, 7.5 wt%)in DT-TiO_2 on hydrogen production performance with 0.6 wt% Pt loading (Fig. S8). The calcination temperature was set at 300 °C with a calcination rate of 2.5 °C /min for 2 hours, followed by natural cooling. The results showed that DT-TiO_2(5.0 wt%) exhibited the best photocatalytic performance, achieving a hydrogen production rate of 10.615 mmol·g^{-1}·h^{-1}. Lower or higher doping amounts reduced the photocatalytic activity, possibly due to excess DT molecules accumulating on the TiO_2 surface, hindering photogenerated charge transport and decreasing photocatalytic performance.

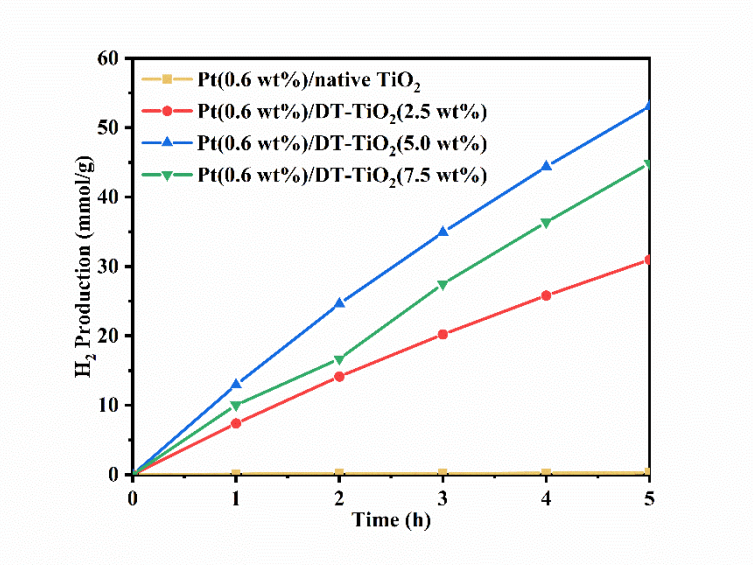

Fig. S8 Hydrogen production performance of DT-TiO_2 with different content of DT dopant.

We then examined the effect of different calcination temperatures on the hydrogen production performance of the entire catalytic system using DT-TiO_2(5.0 wt%) with the same content (5.0 wt%). We included samples without calcination and those calcined at temperatures of 200 °C, 250 °C, 300 °C, and 350 °C, with a fixed heating rate of 5 °C /min. The temperature was allowed to decrease naturally after calcination for 2 hours, and Pt loading was fixed at 1.0 wt%. The results show that under the same conditions, the photocatalytic performance of DT-TiO_2 is optimal at a calcination temperature of 300 °C, which is significantly better than at higher (350 °C) or lower (200 °C) calcination temperatures. This suggests that the appropriate calcination temperature can eliminate impurities while increasing the material's crystallinity (Fig. S9A). Finally, we studied the influence of different heating rates on the hydrogen production performance of the entire catalytic system by screening DT-TiO_2(5.0 wt%) samples with the same content and calcination temperature (300 °C). The results show that the photocatalytic performance of DT-TiO_2 is optimal when the calcination heating rate is 2.5 °C /min (Fig. S9B).

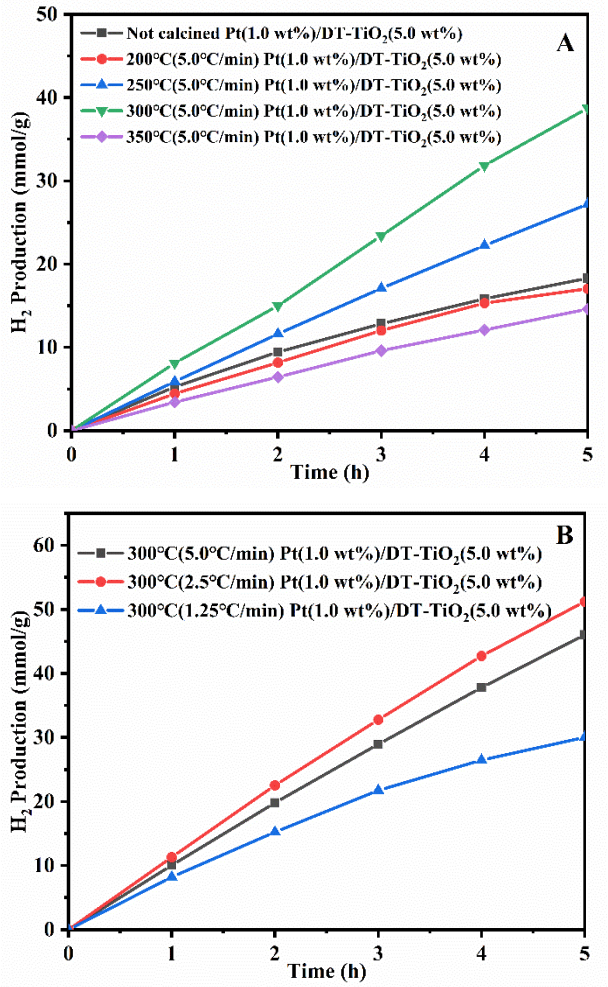

Fig. S9 (A)Hydrogen production performance of DT-TiO_2(5.0 wt%)at different calcination temperatures;(B) Hydrogen production performance of DT-TiO_2 (5.0 wt%) at different calcination rates.

We then investigated the relationship between photocatalytic performance and the co-catalyst. Keeping DT content and calcination method constant, we studied the effect of different Pt loadings on DT-TiO_2(5.0 wt%) hydrogen production performance under visible light. The results revealed that the optimal Pt loading was 0.6 wt%, yielding a hydrogen production rate of 10.6147 $mmol \cdot g^{-1} \cdot h^{-1}$. Excessive loading hindered light absorption and acted as a recombination center for photogenerated electrons and holes, resulting in reduced catalytic activity (Fig. S10). We used ICP-AES to verify the Pt element content in the material, and Table. S1 shows the comparison between theoretical and actual values of Pt loading. The results confirmed that Pt NPs were successfully loaded onto the Pt@DT-TiO_2 composite material, with only minor differences in values.

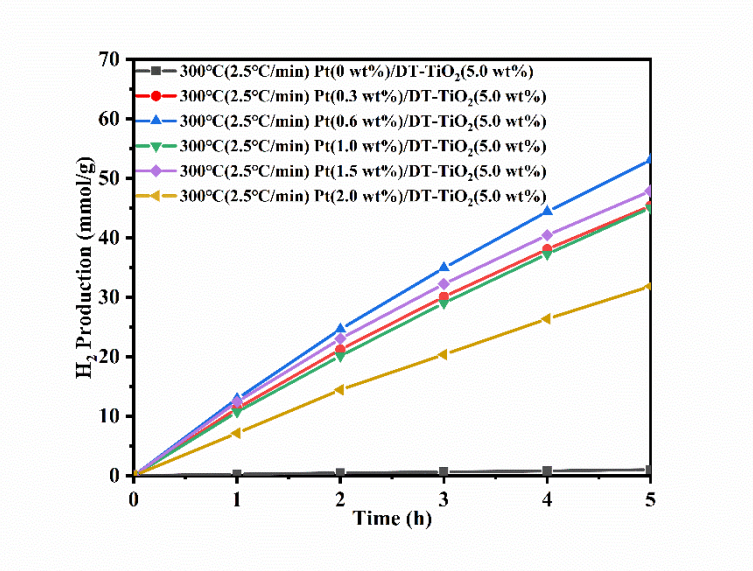

Fig. S10 The effects of different amounts of Pt loading on hydrogen production performance of DT-TiO_2 (5.0 wt%)

Table S1. The amount of Pt NPs of Pt@DT-TiO_2 analysed by ICP-AES.

Sample	Pt content(wt%)
Pt(0.3 wt%)/DT-TiO_2(5.0 wt%)	0.2
Pt(0.6 wt%)/DT-TiO_2(5.0 wt%)	0.5
Pt(1.0 wt%)/DT-TiO_2(5.0 wt%)	1.0
Pt(1.5 wt%)/DT-TiO_2(5.0 wt%)	1.2
Pt(2.0 wt%)/DT-TiO_2(5.0 wt%)	1.6

We tried ethanol as a sacrificial agent and compared it to triethanolamine, but unfortunately ethanol did not work well, so we chose triethanolamine as the sacrificial agent (Fig. S11).We provide comparative data on hydrogen production in the presence of 0.6 wt% Pt of 5 mg, 10 mg and 15 mg DT-TiO_2 photocatalysts (Fig. S12), and the results showed that when the photocatalyst dosage increased from 5 mg to 10 mg, the hydrogen production also increased, but at the photocatalyst dosage of 15 mg, the hydrogen production decreased due to the reduction of light penetration depth in the heterogeneous system and severe light scattering and reflection. Therefore, we chose to perform subsequent photocatalytic hydrogen production performance tests at 10 mg, because the platform region was not limited by diffusion and saturated light absorption.[S5]

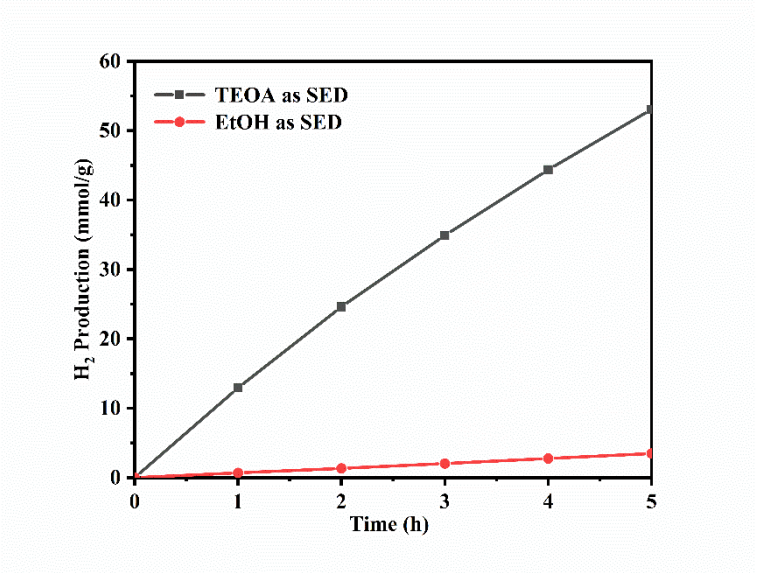

Fig. S11 Selection of different sacrificial agents.

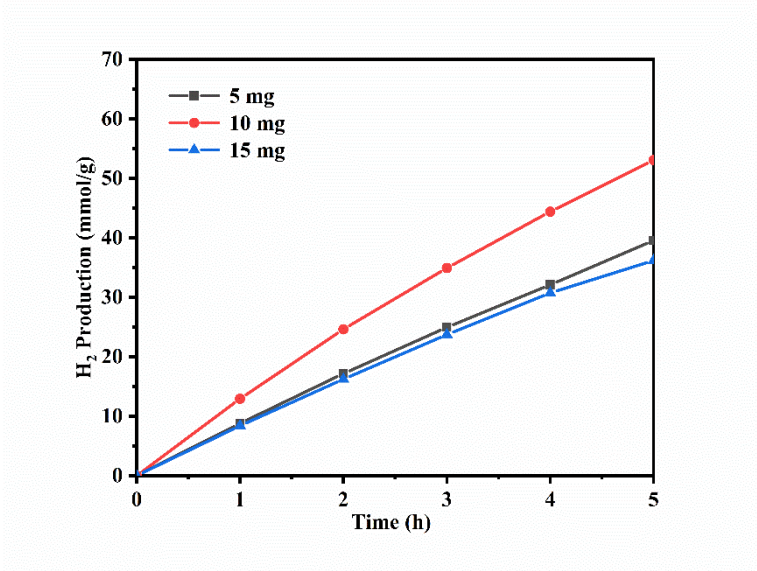

Fig.S12 Dependence of hydrogen production on photocatalyst concentration.

We surveyed some literatures related to dye-sensitized TiO_2 in recent years, and compiled the table according to the relevant data such as dye type, noble metal co-catalyst, light source, wavelength, sacrificial agent, and hydrogen production per hour, to measure the production of the same type of catalyst. hydrogen rate. (Table S2).

Table S2. Comparison of hydrogen production activities of DT-TiO_2 and dye-sensitized TiO_2 photocatalytic systems.

Catalyst	Co-Catalyst	Sacrificial agent	Xenon lamp (W)	Light source (nm)	H_2 Production rate ($\mu mol \cdot g^{-1} \cdot h^{-1}$)	Ref
DT-TiO_2	Pt	TEOA	300	＞400	10615	This work
H_4TTFTB-TiO_2	Pt	TEOA	300	＞400	1452	S6
Thionine-TiO_2	Pt	TEOA	150	＞420	28	S7
DPPCN/TiO_2	Pt	TEOA	400	＞400	12080	S8
DPPCA/TiO_2	Pt	TEOA	400	＞400	8400	S8
Rh B-TiO_2	Co	TEOA	300	＞420	227.3	S9
DEO2-TiO_2	Pt	EDTA	450	＞420	800	S10
P42-TiO_2	Pt	TEOA	300	＞420	745.0	S4
DH1-MC-TiO_2	Pt	TEOA	300	＞420	8910	S11
P5- TiO_2	Pt	TEOA	200	＞420	3079	S12
MW3-TiO_2	Pt	TEOA	300	＞420	4055	S13
HO-TPA-TiO_2	Pt	TEOA	300	＞420	2633	S14
PI-OMe-TiO_2	Pt	TEOA	300	＞420	1190	S15
3C/TiO_2	Pt	TEOA	250	＞420	247	S16
B-Car/TiO_2	Pt	Ascorbic acid	-	＞420	249	S17
DN1-TiO_2	Pt	TEOA	400	＞400	7950	S18
PAN-TiO_2	Pt	Thiogiycolic acid	150	＞420	62	S19
Chl-3-TiO_2	Pt	Ascorbic acid	350	＞400	263	S20
MZ-TiO_2	Cu_2WS_4	TEOA	300	＞420	6340	S21
Eosin Y^+-TiO_2	$Ni(OH)_2$	TEOA	300	＞420	1576	S22
AM-TiO_2	Pt	TEOA	400	＞400	6798	S23
MK2-TiO_2	Pt	TEOA	400	＞400	9448	S23
MZ-341-TiO_2	Cu_2WS_4	TEOA	300	＞420	1406	S21
MZ-235-TiO_2	Cu_2WS_4	TEOA	300	＞420	943	S21
C4BTP-TiO_2	Pt	TEOA	300	＞420	8048	S24

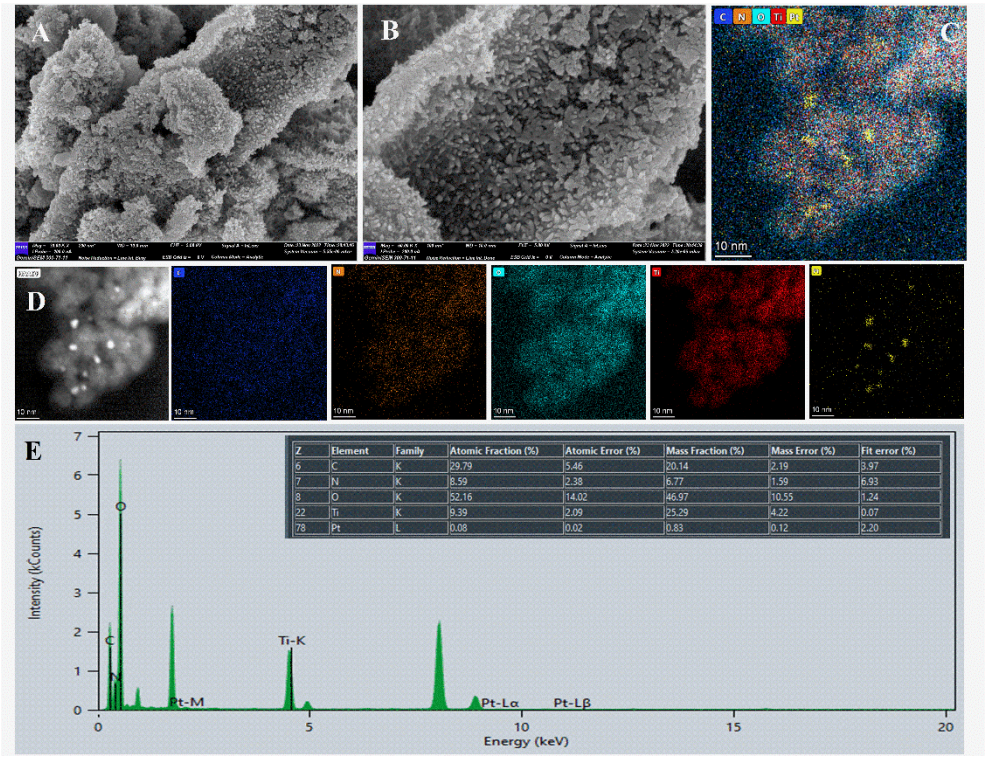

Fig. S13 (A)(B) SEM image of DT-TiO_2 (5.0 wt%); (C) Element mapping and (D) EDX analysis of Pt (0.6 wt%)/DT-TiO_2 (5.0 wt%).

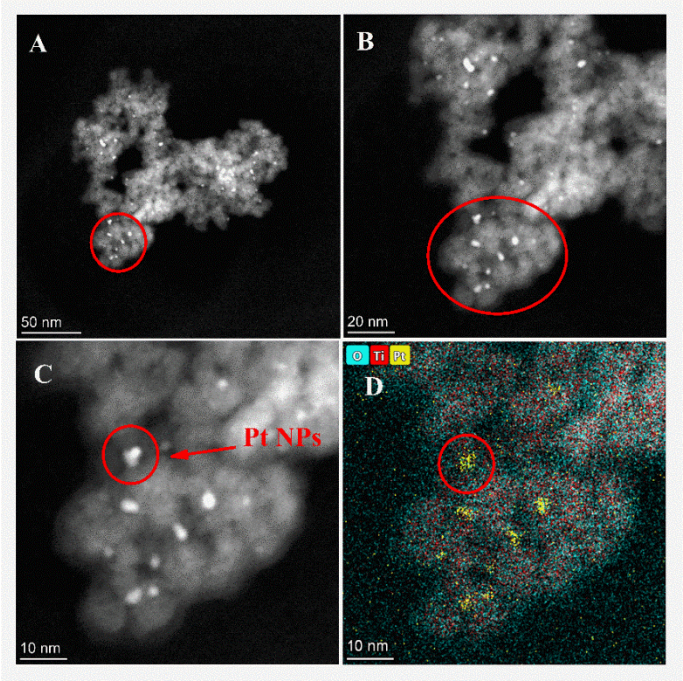

Fig. S14 HAADF-STEM of Pt(0.6 wt%)/DT-TiO_2(5.0 wt%).

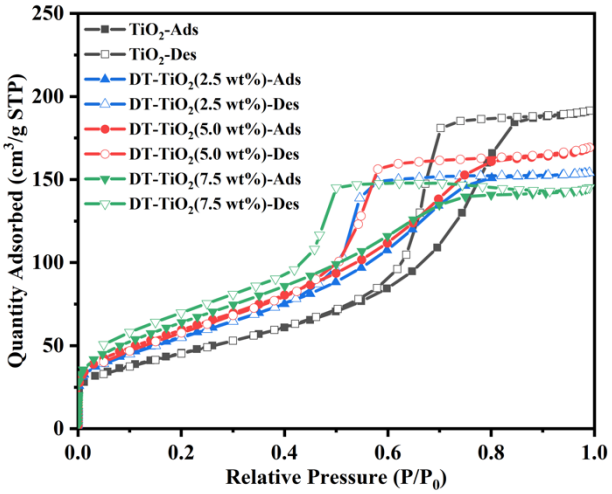

Fig. S15 The N_2 adsorption and desorption measured of TiO_2 and DT-TiO_2 (2.5/5.0/7.5 wt%) at 77K.

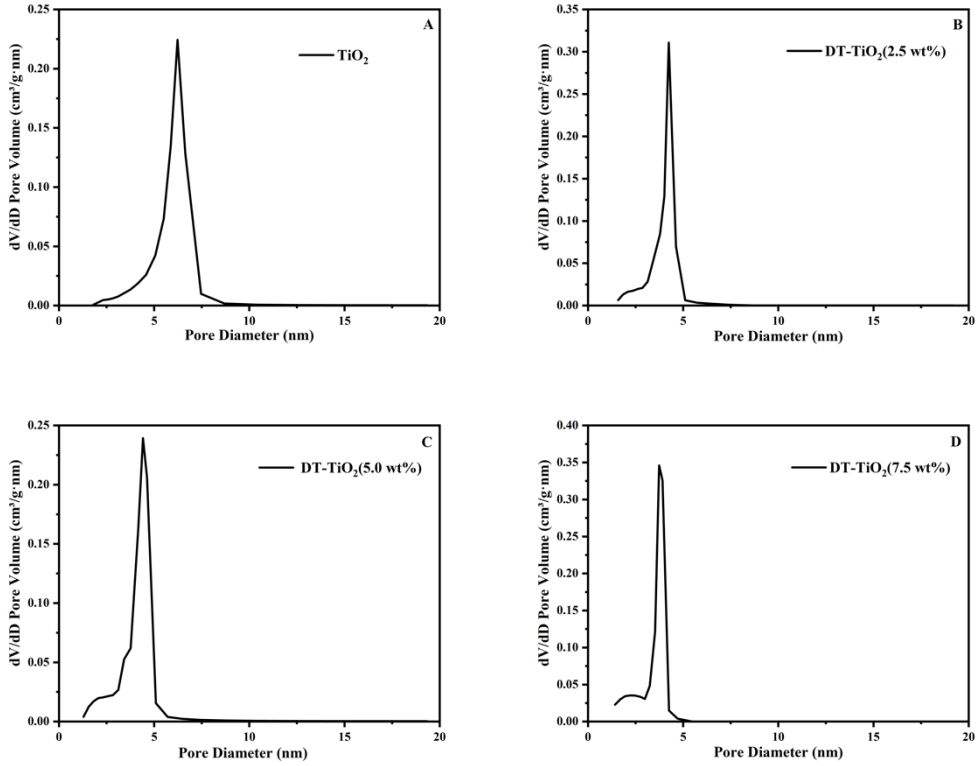

Fig. S16 The pore size distribution of TiO_2 and DT-TiO_2 (2.5/5.0/7.5 wt%).

Table S3. BET surface area, pore diameter and pore volume of TiO_2 and DT-TiO_2 (2.5/5.0/7.5 wt%).

Sample	Surface area (m^2/g)	Pore size (nm)	Pore volume (cm^3/g)
TiO_2	166.461	7.118	0.296
DT-TiO_2(2.5 wt%)	204.249	4.672	0.239
DT-TiO_2(5.0 wt%)	219.910	4.765	0.262
DT-TiO_2(7.5 wt%)	237.793	3.777	0.225

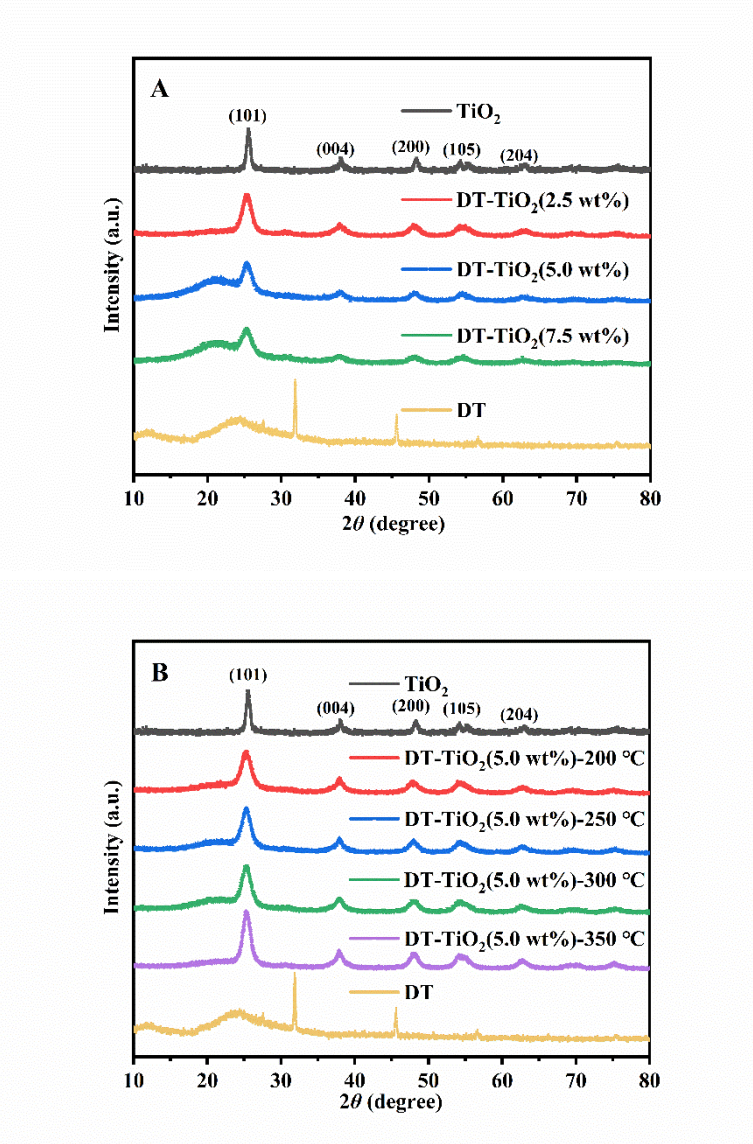

Fig. S17 XRD spectra of (A)DT-TiO_2 with different DT contents under calcination conditions at 300 °C (2.5 °C /min) and (B) **DT-TiO_2 (5.0 wt%) at different calcination temperatures** (200 ℃, 250 ℃, 300 ℃, 350 ℃)

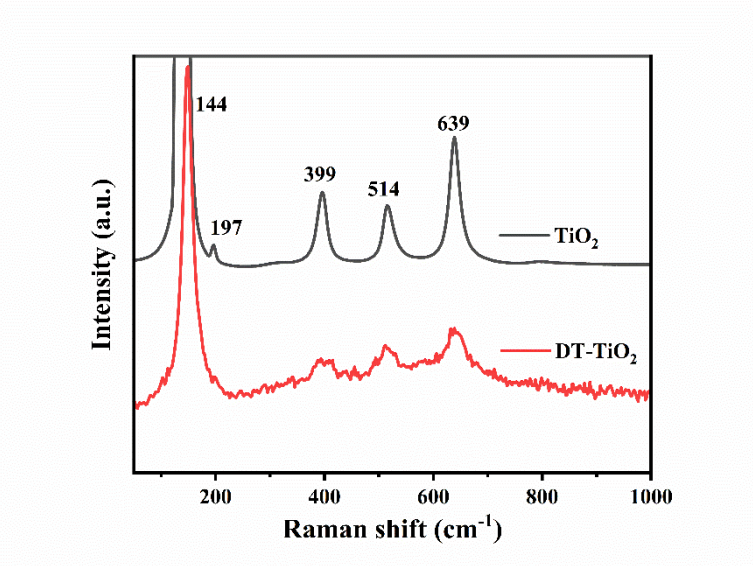

Fig. S18 Raman spectra of TiO_2 and DT-TiO_2 (5.0 wt%).

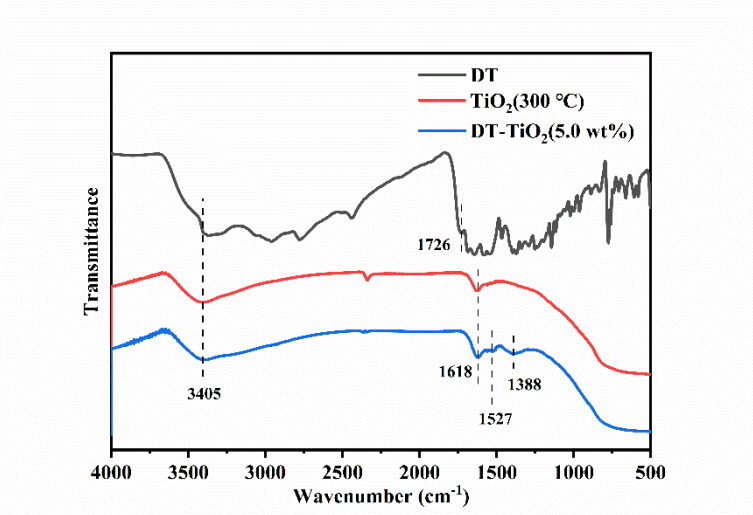

Fig. S19 The FT-IR spectra of DT, TiO_2 and DT-TiO_2 (5.0 wt%).

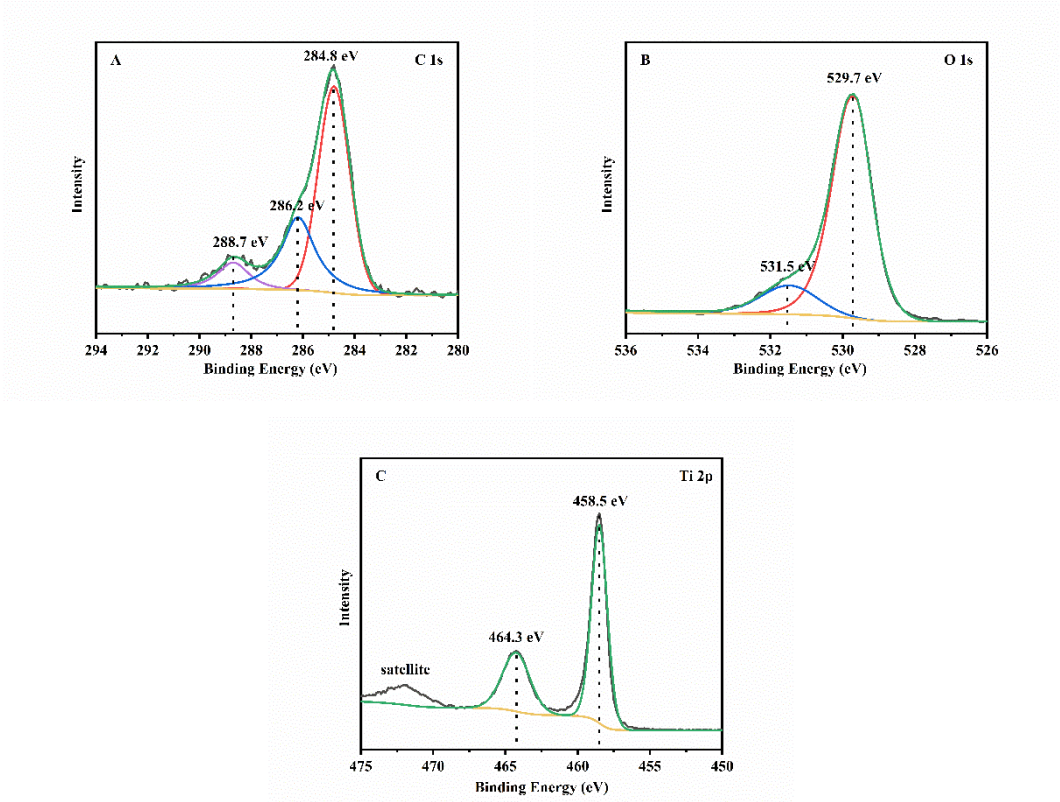

Fig. S20 X-ray of photoelectron spectra of C,O and Ti in TiO_2. Atomic ratio of Ti : O = 26% : 50% ≈ 1 : 2.

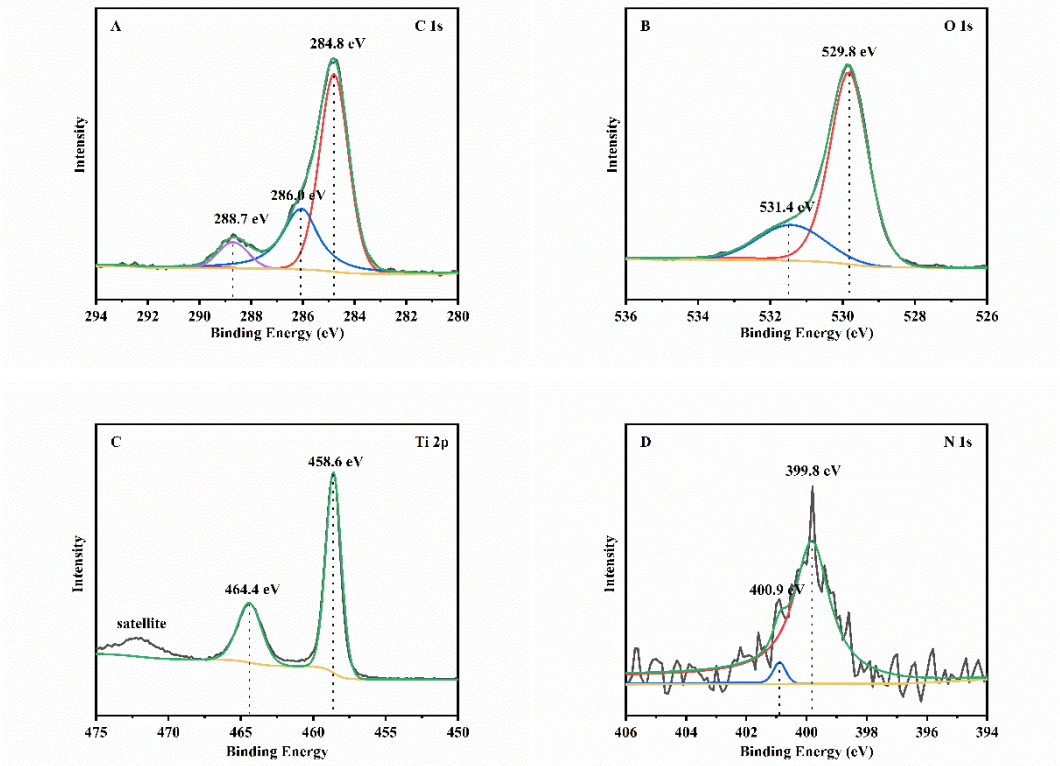

Fig. S21 X-ray of photoelectron spectra of C,O,N and Ti in DT-TiO_2(5.0 wt%). Atomic ratio of Ti : O : C : N = 42% : 47% : 10% : 1%.

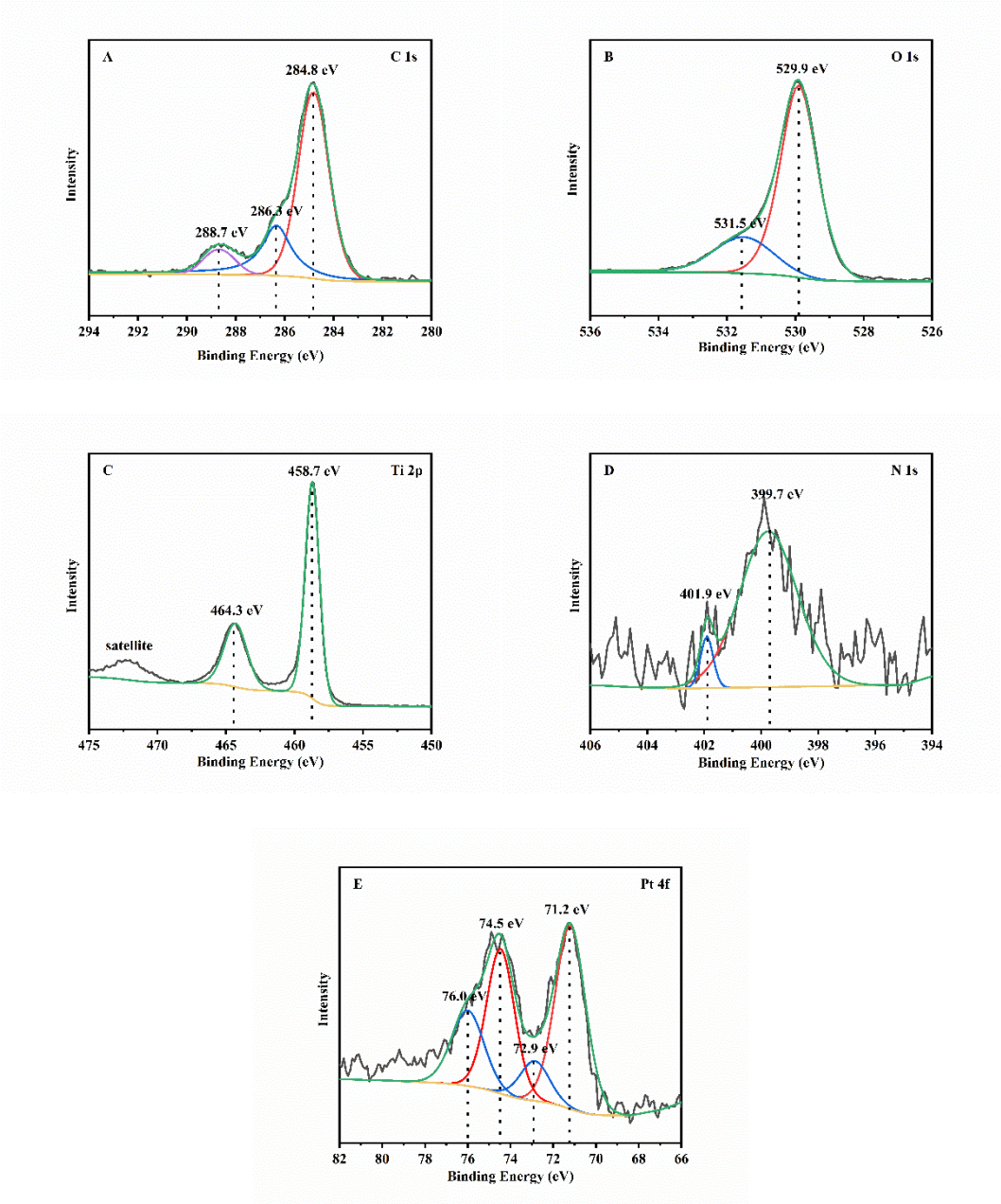

Fig. S22 X-ray of photoelectron spectra of C,O,N,Ti and Pt in Pt(0.6 wt%)/DT-TiO_2(5.0 wt%).

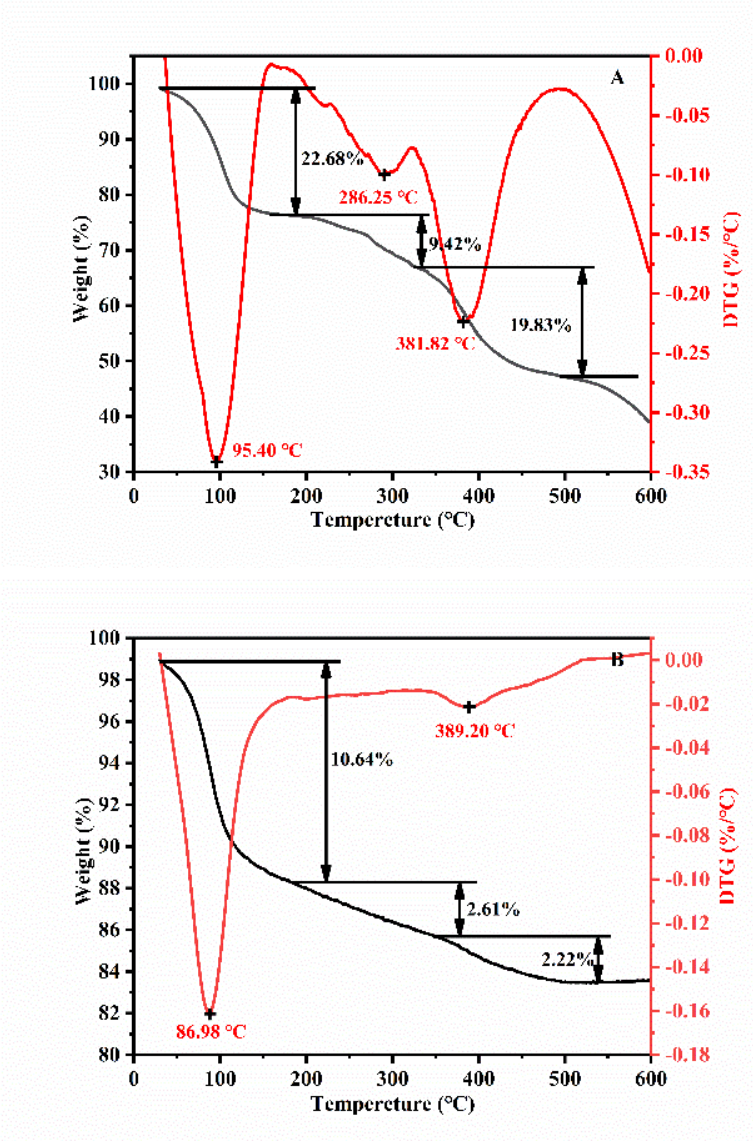

Fig. S23 Thermogravimetric analysis of (A) DT and (B) DT-TiO_2 (5.0 wt%) materials, the temperature gradient was from 30 ℃ to 600 ℃ at a heating rate at 10 ℃/min. The humidity of the test environment was about 76%.

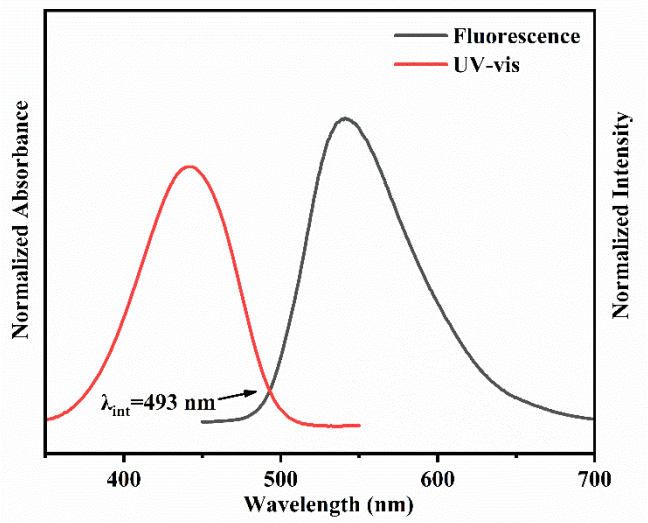

Fig. S24 UV-vis and Fluorescence Spectra of DT.

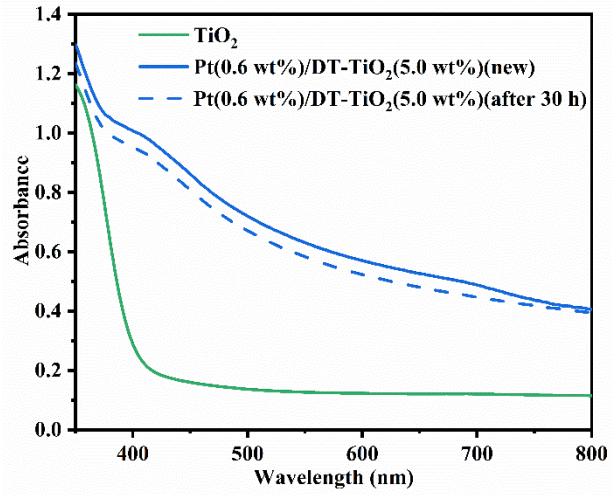

Fig. S25 UV-vis absorption spectra before and after 30 hours.

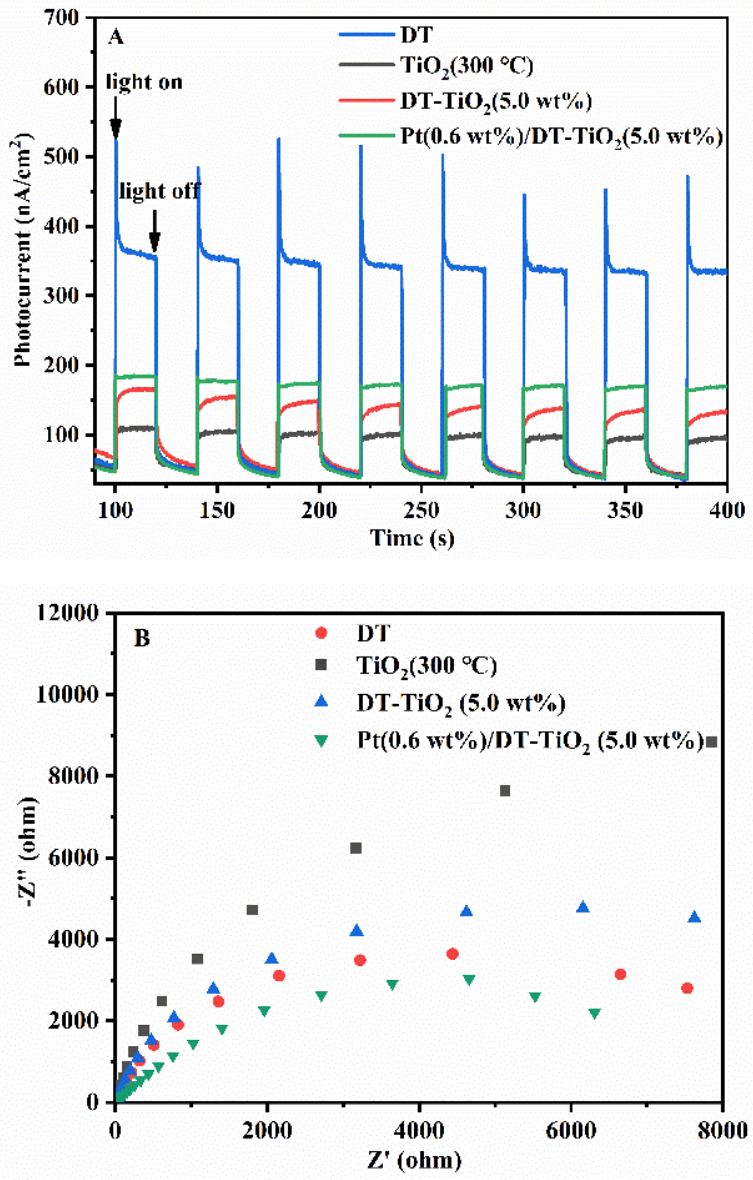

Fig. S26 (A)Instantaneous current (I-t) diagram and (B) electrochemical impedance (EIS) diagram of DT, TiO_2 ,DT-TiO_2 and Pt(0.6 wt%)/DT-TiO_2(5.0 wt%).

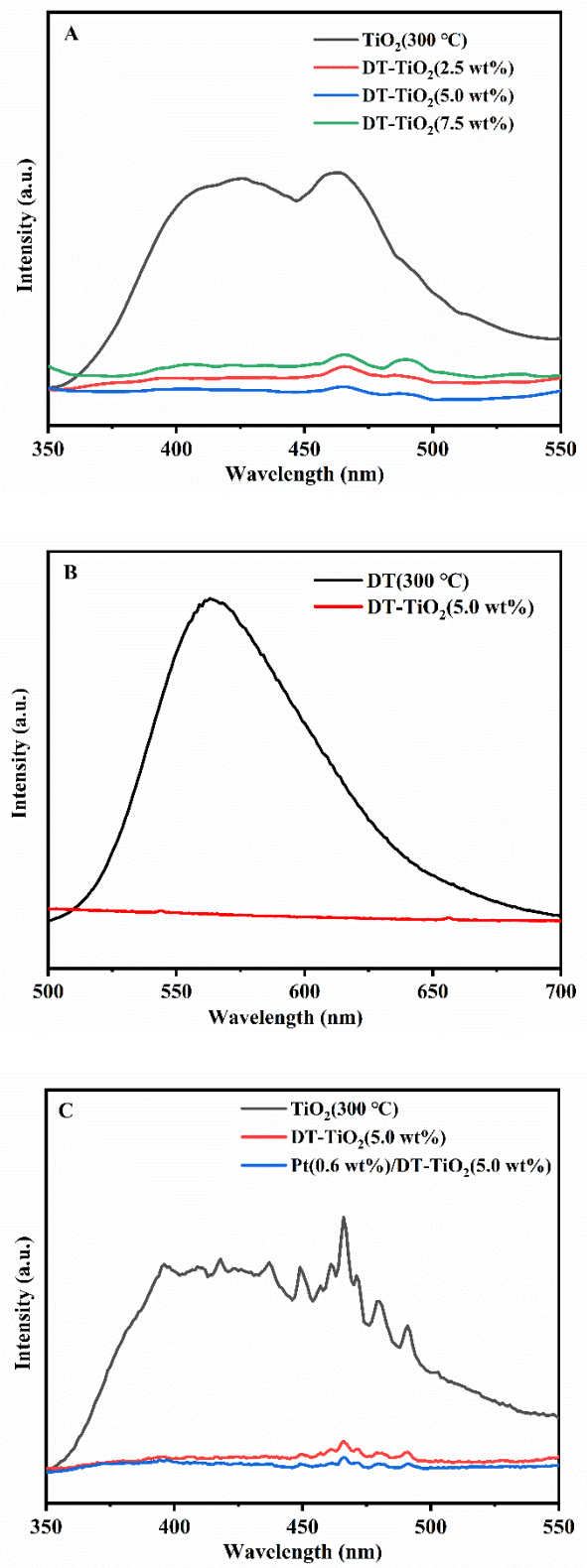

Fig. S27 Solid state fluorescence emission spectra of (A)TiO_2 and DT-TiO_2 (2.5/5.0/7.5 wt%) (B) DT and DT-TiO_2(5.0 wt%) and (C) **TiO_2, DT-TiO_2(5.0 wt%) and Pt(0.6 wt%)/ DT-TiO_2(5.0 wt%).**

Table S4. AQY results of DT-TiO_2(5.0 wt%) after 1h irradiation under 405 nm, 450 nm LED light source.

Sample	Pt(0.6 wt%)/DT-TiO_2(5.0 wt%)	Pt(0.6 wt%)/DT-TiO_2(5.0 wt%)
Wavelength (nm)	405	450
AQY	1.94	1.44

AQY = (the number of hydrogen molecules produced by the reaction × 2 / number of incident photons) × 100%.

REFERENCES

S1. W. L. Turnbull, E. Murrell, M. Bulcan-Gnirss, M. Majeed, M. Milne and L. G. Luyt, *Dalton Trans*, 2019, **48**, 14077-14084.

S2. Q. Lin, G. F. Gong, Y. Q. Fan, Y. Y. Chen, J. Wang, X. W. Guan, J. Liu, Y. M. Zhang, H. Yao and T. B. Wei, *Chem Commun (Camb)*, 2019, **55**, 3247-3250.

S3. Z. Qian, C. A. Rhodes, L. C. McCroskey, J. Wen, G. Appiah-Kubi, D. J. Wang, D. C. Guttridge and D. Pei, *Angew Chem Int Ed Engl*, 2017, **56**, 1525-1529.

S4. F. Jing, Y. Guo, B. Li, Y.-F. Chen, C. Jia and J. Li, *Chinese Chemical Letters*, 2022, **33**, 1303-1307.

S5. J. M. Buriak, *Chemistry of Materials*, 2017, **29**, 1-2.

S6. M. Wang, S. Su, X. Zhong, D. Kong, B. Li, Y. Song, C. Jia and Y. Chen, *Nanomaterials (Basel)*, 2022, **12**, 1918.

S7. D. Chatterjee, *Catalysis Communications*, 2010, **11**, 336-339.

S8. K. Narayanaswamy, A. Tiwari, I. Mondal, U. Pal, S. Niveditha, K. Bhanuprakash and S. P. Singh, *Phys Chem Chem Phys*, 2015, **17**, 13710-13718.

S9. T. T. Le, M. S. Akhtar, D. M. Park, J. C. Lee and O. B. Yang, *Applied Catalysis B: Environmental*, 2012, **111-112**, 397-401.

S10. W. S. Han, K. R. Wee, H. Y. Kim, C. Pac, Y. Nabetani, D. Yamamoto, T. Shimada, H. Inoue, H. Choi, K. Cho and S. O. Kang, *Chemistry*, 2012, **18**, 15368-15381.

S11. J. F. Huang, Y. Lei, L. M. Xiao, X. L. Chen, Y. H. Zhong, S. Qin and J. M. Liu, *ChemSusChem*, 2020, **13**, 1037-1043.

S12. J. Lee, J. Kwak, K. C. Ko, J. H. Park, J. H. Ko, N. Park, E. Kim, D. H. Ryu, T. K. Ahn, J. Y. Lee and S. U. Son, *Chem Commun (Camb)*, 2012, **48**, 11431-11433.

S13. M. Watanabe, H. Hagiwara, A. Iribe, Y. Ogata, K. Shiomi, A. Staykov, S. Ida, K. Tanaka and T. Ishihara, *J. Mater. Chem. A*, 2014, **2**, 12952-12961.

S14. Y.-F. Chen, J.-F. Huang, M.-H. Shen, J.-M. Liu, L.-B. Huang, Y.-H. Zhong, S. Qin, J. Guo and C.-Y. Su, *Journal of Materials Chemistry A*, 2019, **7**, 19852-19861.

S15. H. Wu, M. Wang, F. Jing, D. Kong, Y. Chen, C. Jia and J. Li, *Chinese Chemical Letters*, 2022, **33**, 1983-1987.

S16. H. Lai, X. Liu, F. Zeng, G. Peng, J. Li and Z. Yi, *ACS Omega*, 2020, **5**, 2027-2033.

S17. X.-F. Shen, M. Watanabe, A. Takagaki, J. T. Song and T. Ishihara, *Catalysts*, 2020, **10**.

S18. A. Tiwari and U. Pal, *International Journal of Hydrogen Energy*, 2015, **40**, 9069-9079.

S19. X. Liu, H. Lai, J. Li, G. Peng, Z. Yi, R. Zeng, M. Wang and Z. Liu, *International Journal of*

Hydrogen Energy, 2019, **44**, 4698-4706.

S20. Y. Sun, X.-F. Wang, G. Chen, C.-H. Zhan, O. Kitao, H. Tamiaki and S.-i. Sasaki, *International Journal of Hydrogen Energy*, 2017, **42**, 15731-15738.

S21. E. Aslan, M. K. Gonce, M. Z. Yigit, A. Sarilmaz, E. Stathatos, F. Ozel, M. Can and I. H. Patir, *Applied Catalysis B: Environmental*, 2017, **210**, 320-327.

S22. Z. Yan, X. Yu, Y. Zhang, H. Jia, Z. Sun and P. Du, *Applied Catalysis B: Environmental*, 2014, **160-161**, 173-178.

S23. A. Kumari, I. Mondal and U. Pal, *New Journal of Chemistry*, 2015, **39**, 713-720.

S24. Y.-H. Zhong, Y. Lei, J.-F. Huang, L.-M. Xiao, X.-L. Chen, T. Luo, S. Qin, J. Guo and J.-M. Liu, *Journal of Materials Chemistry A*, 2020, **8**, 8883-8891.